Zinc Barbiturate Complexes with Bidentate N-Donor Ligands: Syntheses, Crystal Structures, Spectroscopic, Thermal and Voltammetric Studies

Fatih Yilmaz[a], Veysel T. Yilmaz[b], Ender Bicer[b], and Orhan Büyükgüngör[c]

[a] Department of Chemistry, Rize Faculty of Arts and Sciences, Karadeniz Technical University, Rize, Turkey
[b] Department of Chemistry, Faculty of Arts and Sciences, Ondokuz Mayis University, 55139 Kurupelit, Samsun, Turkey
[c] Department of Physics, Faculty of Arts and Sciences, Ondokuz Mayis University, 55139 Kurupelit, Samsun, Turkey

Reprint requests to Prof. Dr. V. T. Yilmaz. E-mail:vtyilmaz@omu.edu.tr

Z. Naturforsch. **61b,** 275 – 280 (2006); received December 15, 2005

Two new bis(5,5–diethylbarbiturato) (barb) complexes of zinc, $[Zn(barb)_2(en)]$ (**1**) and $[Zn(barb)_2(bpy)] \cdot H_2O$ (**2**) [en = ethylenediamine, bpy = 2,2'-bipyridine], have been prepared and characterized by elemental analysis, IR spectroscopy, thermal analysis and single crystal X-ray diffraction. Complexes **1** and **2** crystallize in monoclinic space groups. The zinc(II) ions in complex **1** are tetrahedrally coordinated by two barb and an en ligand. The barb ligands are N-coordinated while the en ligand acts as a bidentate chelating ligand. One carbonyl oxygen atom of each barb ligands in complex **2** participates in the bonding with the zinc ion with remarkably long Zn–O bonds resulting in a highly distorted octahedral geometry. Molecules of complex **1** are connected *via* N–H···O hydrogen bonds, involving hydrogen atoms of both barb and en ligands, while molecules of complex **2** are linked by N–H···O and O–H···O hydrogen bonds and also aromatic π(bpy)···π(bpy) stacking interactions. The voltammetric behavior of complexes **1** and **2** was investigated in aqueous solution by cyclic voltammetry using a NH_3/NH_4Cl buffer. The cyclic voltammogram of **1** shows a cathodic peak at −1.260 V and an anodic peak at −1.068 V due to a quasi-reversible two-electron process. Complex **2** yields two reduction peaks at −1.312 and −1.412 V. The former corresponds to a quasi-reversible electrode process of the zinc(II) ions in complex **2**, while the latter is attributed to the reduction of the coordinated bpy ligands.

Key words: Barbiturate, Ethylenediamine, 2,2'-Dipyridyl, Zinc, Crystal Structure

Introduction

Barbiturates are widely used as sedative hypnotic drugs and are also employed for anesthesia since their discovery at the beginning of the last century [1]. In 1931, Zwicker [2] first prepared a crystalline adduct of a commonly used barbiturate [chemically known as 5,5-diethylbarbituric acid (barbH), also known as barbital, veronal or diemal] by reaction of this barbiturate with an aqueous solution of copper sulphate in pyridine, and assigned it the formula $[Cu(barb)_2(py)_2]$. Owing to their potential use in clinical detection and estimation of these drugs, several such metal complexes of barbiturates have been prepared [3, 4].

From the viewpoint of coordination chemistry, the presence of several potential donor atoms such as two amine nitrogen and three carbonyl oxygen atoms makes barbiturates very interesting and polyfunctional ligands. Among barbiturates, barbital (barbH) is chemically the simplest derivative used especially in the form of its soluble salts such as Na(barb). Only two zinc-barb complexes, $[Zn(barb)_2(im)_2]$ (imidazole) [5] and $[Zn(barb)_2(pic)_2]$ (pic = picoline) [6], have been reported. In these complexes, the barbiturate ligand is deprotonated and coordinated through the negatively charged N atom.

Recently, we have reported the synthesis and characterization of the new copper and cadmium complexes of barb with en, namely *cis*-$[Cu(barb)_2(en)]$ [7] and $\{[Cd(barb)_2(\mu\text{-en})] \cdot 2H_2O\}_n$ [7]. The barb ligand in both complexes acts as a bidentate chelating ligand *via* the negatively charged imino N atom and one of the carbonyl O atoms adjacent to the imino N atom. In this paper, we report the syntheses, struc-

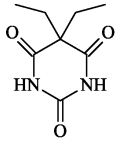

barbH

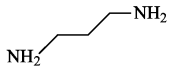

en

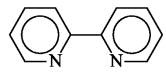

bpy

tures, thermal behaviors, and redox properties of two new zinc-barb complexes with the bidentate N-donor chelating ligands en and 2,2'-dipyridyl (bpy), namely $[Zn(barb)_2(en)]$ (**1**) and $[Zn(barb)_2(bpy)] \cdot H_2O$ (**2**).

Results and Discussion

Synthesis

The reaction of Na(barb) with $Zn(NO_3)_2$ in water in the presence of en or bpy at r. t. yielded the title complexes, bis(5,5-diethylbarbiturato)(ethylenediamine)zinc(II) (**1**) and bis(5,5-diethylbarbiturato)(2,2'-dipyridyl)zinc(II) (**2**) in high yields. The analytical data (C, H, and N) are consistent with the expected formulations of these complexes. The title complexes are non-hygroscopic and stable in air at room temperature. Both complexes are highly soluble in the mixture of water and 2-propanol (5:1), but slightly soluble in water, methanol, ethanol, and 2-propanol. They do not melt, but decompose at 265 and 72 °C, respectively.

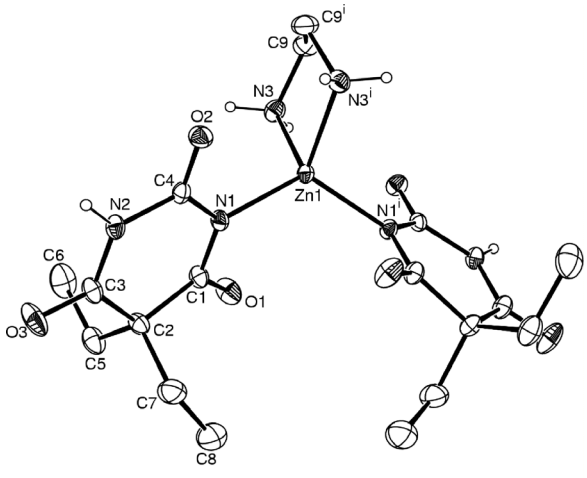

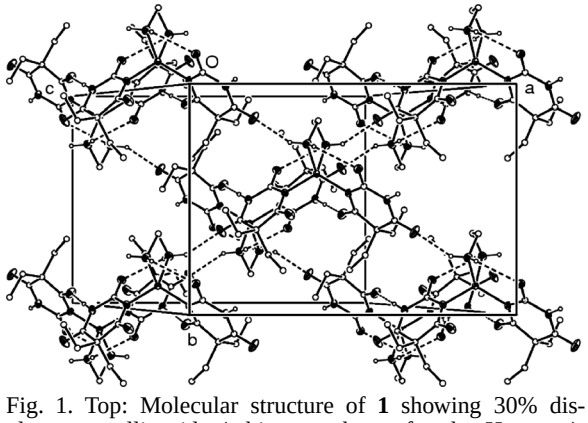

Fig. 1. Top: Molecular structure of **1** showing 30% displacement ellipsoids (arbitrary spheres for the H atoms). C–H hydrogen atoms are omitted for clarity. Symmetry code [i] $1-x, y, 3/2-z$. Bottom: Packing diagram of **1**.

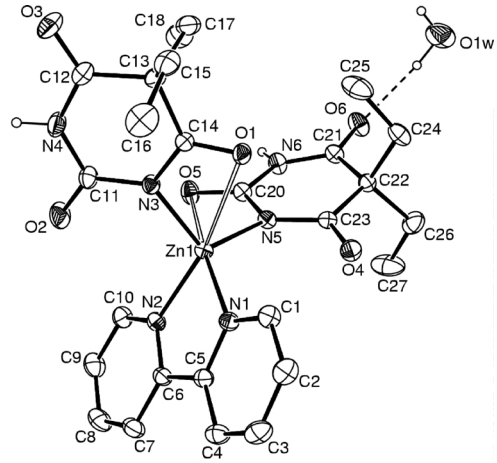

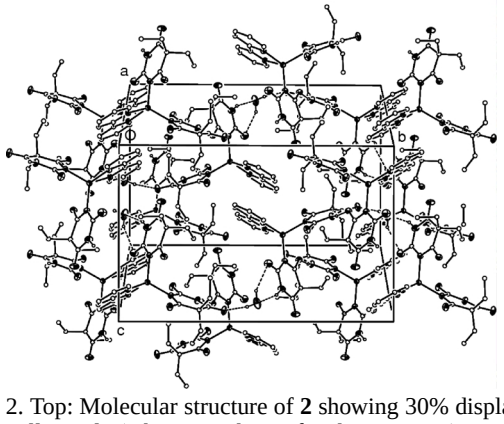

Fig. 2. Top: Molecular structure of **2** showing 30% displacement ellipsoids (arbitrary spheres for the H atoms). Hydrogen bonds are indicated by dashed lines and open bonds indicate weak bonding interactions. C–H hydrogen atoms are omitted for clarity. Bottom: Packing diagram of **2**.

Description of the crystals structures

Figs 1 and 2 show the molecular structures of **1** and **2** with atom labeling, respectively. Selected bond distances and angles are listed in Tables 1 and 2, respectively, together with the hydrogen bonding geometry.

Table 1. Selected bond lengths and angles, and hydrogen bonding geometry of **1**[a].

Bond lengths (Å) and angles (°)			
Zn1–N1	1.980(2)	N1–Zn1–N1^{i}	119.26(11)
Zn1–N3	2.068(2)	N1–Zn1– N3	106.91(8)
		N1–Zn1– N3^{i}	117.03(8)
		N3–Zn1– N3^{i}	85.04(13)

Hydrogen bonds

D–H···A	D–H (Å)	H···A (Å)	D···A (Å)	D–H···A (°)
N2-H2···O1^{ii}	0.86	2.07	2.917(3)	167
N3-H3A···O2^{i}	0.90	2.54	3.058(3)	117
N3-H3B···O3^{iii}	0.90	2.24	3.062(3)	151

[a] Symmetry operations: [i] $1-x,\ y,\ 3/2-z$; [ii] $x,\ 1-y,\ z-3/2$; [iii] $3/2-x,\ 1/2+y,\ 3/2-z$.

Table 2. Selected bond lengths and angles, and the hydrogen bonding geometry of **2**[a].

Bond lengths (Å) and angles (°)			
Zn1–N1	2.051(1)	N1–Zn1–N2	79.91(6)
Zn1–N2	2.063(1)	N1–Zn1–N3	112.35(6)
Zn1–N3	1.982(2)	N1–Zn1–N5	117.23(6)
Zn1–N5	1.978(1)	N2–Zn1–N3	114.92(6)
Zn1–O1	2.813(1)	N2–Zn1–N5	112.93(6)
Zn1–O5	2.839(1)	N3–Zn1–N5	114.92(6)

Hydrogen bonds

D–H···A	D–H (Å)	H···A (Å)	D···A (Å)	D–H···A (°)
O1W–H30···O6	0.89(3)	1.95(3)	2.833(3)	171(6)
O1W–H31···O2^{i}	0.90(3)	2.55(6)	3.272(3)	137(7)
N6–H6···O1^{ii}	0.86	1.98	2.829(2)	172
N4-H41···O1W^{iii}	0.86	2.11	2.938(3)	161

[a] Symmetry operations: [i] $1/2-x,\ 1/2+y,\ 3/2-z$; [ii] $x-1/2,\ 3/2-y,\ z-1/2$; [iii] $1/2-x,\ y-1/2,\ 3/2-z$.

Both complexes crystallize in the monoclinic crystal system.

The molecules in complex **1** have two-fold crystallographic symmetry. The zinc(II) ion is tetrahedrally coordinated by an en ligand and two barb anions, forming a distorted tetrahedral ZnN_4 core. The en ligand behaves as a bidentate N,N' donor chelating ligand, forming a five-membered chelate ring, while each barb ligand is *N*-coordinated. The bite angle of the en ligand is 85.04(13)° and significantly contributes to the distortion of the coordination geometry around the zinc(II) ion in **1**. In complex **2**, the coordination geometry around zinc(II) is basically a distorted tetrahedron determined by the deprotonated nitrogen atoms of two barb anions and by two nitrogen atoms of a neutral bpy ligand. However, in contrast to **1**, one carbonyl oxygen atom of each barb ligand in complex **2** also participates in the bonding with the zinc(II) ion with remarkably long Zn–O bonds (around 2.83 Å). Consequently, the tetrahedral ZnN_4 array is extended to a highly distorted ZnN_4O_2 octahedral geometry. The significant distortion is evident from the angles in the coordination polyhedron (see Table 2), the highest deviation being observed in the bite angle [51.64(8)°] of barb. The barb ligands are located in *cis* positions of the octahedron and behave as bidentate chelating ligand through the negatively charged N and one of the carbonyl O atoms, while the bpy ligand acts as a bidentate ligand forming a five-membered chelate ring. A similar coordination mode of barb was also observed in *cis*-[Cu(barb)$_2$(en)] [7].

The Zn–N_{barb} bond distances in complexes **1** and **2** are almost identical with an average value of 1.98 Å and are in good agreement with the corresponding distances reported for [Zn(barb)$_2$(im)$_2$] at 2.009(2) Å [5], and [Zn(barb)$_2$(pic)$_2$] at 1.987(3) and 2.006(3) Å [6]. The Zn–$N_{en\ or\ bpy}$ bond distances are similar to the Zn–N_{barb} bond distances. The two Zn–O bond distances in complex **2** are much longer than the analogous bonds found in *cis*-[Cu(barb)$_2$(en)], 2.645(2) Å [7], and [Cu(barb)$_2$(py)$_2$], 2.723(5) Å [8].

The pyrimidine rings of the barb ligands in complexes **1** and **2** are essentially planar and the three carbonyl groups are not significantly displaced from the mean planes of the rings. Conformation, bond lengths and angles of the barb ligands are similar to those of the barb ion [9, 10]. In complex **1**, the dihedral angle between the two barb mean planes is 79.00(5)°. In complex **2**, the mean planes of barb1 with atom N3 and barb2 with atom N5 are nearly perpendicular to each other with a dihedral angle of 83.38(6)°. The py rings within the bpy ligand are slightly tilted by about 1.3°, and the dihedral angles between bpy and barb1, and bpy and barb2, are 58.30(6) and 50.83(4)°, respectively. Packing diagrams of both complexes are shown in Figs 1 and 2. The molecules of complex **1** are connected by N–H···O hydrogen bonds, involving hydrogen atoms of both barb and en ligands. In the structure of complex **2**, the molecules interact with each other *via* N–H···O and O–H···O hydrogen bonds (see Table 2 and Fig. 2). Furthermore, weak aromatic π(bpy)···π(bpy) stacking interactions [$C_g\cdots C_g^{i} = 3.951$ Å; (i) $1-x,\ 1-y,\ 1-z$] and C–H···π(bpy) interactions [C–H···$C_g^{i} = 3.162$ Å; (i) $1-x,\ 1-y,\ -z$] help to reinforce crystal structure.

IR spectra

The most characteristic IR bands of complexes **1** and **2** are given in Table 3. The strong absorption bands in the frequency range 3300 – 3370 cm^{-1} cor-

Table 3. Selected IR spectral data[a] for **1** and **2**.

Assignments	**1**	**2**
ν(OH)	–	3490s,br
$\nu(NH)_{co-ligand}$	3370vs, 3300s	–
$\nu(NH)_{barb}$	3208s,br	3155s
ν(CH)	2967m, 2882w	3047m, 2975m
ν(CO)	1692vs, 1625vs	1687vs, 1633vs, 1600vs
ν(CH)	1437s	1452vs
ν(CN)	1263vs	1263vs

[a] Frequencies in cm^{-1}. b = broad; w = weak; vs = very strong; s = strong; m = medium.

respond to the ν(NH) vibrations of the en ligands, while the strong and broad band centered at 3490 cm^{-1} is assigned to the ν(O–H) vibration of the hydrogen-bonded water molecule. The strong and broad absorption bands at 3280 and 3155 cm^{-1} indicate the presence of the NH groups of the barb ligands in complexes **1** and **2**, respectively. The weak bands around 2882 and 3047 cm^{-1} are characteristic of the ν(CH) vibrations. The stretching vibrations of the carbonyl groups in **1** appear as two very strong absorption bands at 1692 and 1625 cm^{-1}. The carbonyl frequency region in the spectra of **2** differs from that of **1**, since as discussed above, some of the carbonyl groups of the barb ligands participate in bonding. Three sharp absorption bands in the frequency range 1600 – 1687 cm^{-1} characterize vibrations of the carbonyl groups of barb in complex **2**. The bands with strong intensity between 1435 and 1452 cm^{-1} correspond to the C–H deformation vibrations and the very strong band centred at 1263 cm^{-1} is attributed to the C–N stretching vibrations [11].

Thermal analysis

The thermal decomposition behavior of the title complexes was followed up to 800 °C in a static atmosphere of air. Complex **1** is thermally stable up to 265 °C at which temperature it begins to decompose. The decomposition stage between 265 and 306 °C corresponds to removal of the en ligand with a mass loss of 11.9% (calcd. 12.2%). The TG curve shows that the rest of the complex undergoes a continuous mass loss. The DTA curve presents an endothermic peak at 373 °C and two highly exothermic peaks at 410 and 488 °C, which may be attributed to the decomposition of the barb ligands. The decomposition of **1** is complete at 522 °C and the total experimental mass loss value of 82.3% agrees well with the calculated value 83.5%, assuming that the remaining solid residue is ZnO.

Complex **2** is dehydrated in the temperature range 72 – 108 °C. The experimental mass loss of 3.1% for the dehydration stage is consistent with the calculated value of 3.0%. The anhydrous complex starts to decompose at 253 °C and shows a two-step distinct decomposition process. However, mass loss calculations showed that each step does not correspond to elimination of a specific ligand, indicating that the decomposition processes of both bpy and barb ligands overlap to some extend. An endothermic DTA peak at 282 °C is attributed to removal of bpy, while an endothermic peak at 416 °C and two highly exothermic peaks at 443 and 494 °C are due to the degradation of the barb ligands. Total mass loss of 84.4 (total calcd. 86.6%) suggests a ZnO bertolide deficienct in oxygen.

Voltammetric behavior

No voltammetric signal for Na(barb) and en was observed in the selected potential range (from −0.6 to −1.6 V). Studies on the electrochemical behavior of barb and other barbituric acid derivatives have already been reported in the literature [12 – 14]. Specifically, barbituric acid gives a wave at +0.0 V in the borate medium (pH 9.3) [15], whereas barbH exhibits a wave at +0.04 V in the same medium [16].

The cyclic voltammogram of **1** shows a cathodic peak at −1.260 V and an anodic peak at −1.068 V (Fig. 3). As can be seen in Fig. 3, the peak current ratio (I_{pc}/I_{pa}) is 0.84. ΔE_p is greater than $59/n$ mV, where n is the number of electrons transferred, ranging from 160 to 204 mV, and increases with increasing scan rate. Therefore, the electron transfer process is not in equilibrium and shown to be slow. The peak current changes with the scan rate v. The linear equation of the $\log I_p - \log v$ relationship for the cathodic peak, and its slope value of 0.54 indicate that the reduction process is diffusion-controlled. The cathodic peak potential shifts slightly negative potentials with increasing scan rate. The peak couple in Fig. 3 can be attributed to the electrode reaction of the complexed zinc(II) ion within a quasi-reversible two-electron process.

The voltammetric behavior of free bpy was examined to obtain more information on the reduction process of complex **2**. The cyclic voltammogram of bpy is shown in Fig. 3. By scanning the potential from −0.7 to −1.7 V, two cathodic peaks were observed at −1.422 and −1.648 V, respectively. Upon a reverse scan, an anodic peak appeared at −1.385 V (Fig. 3). The peak current ratio I_{pa}/I_{pc} of the pair of anodic (at −1.385 V) and cathodic (at −1.422 V) peaks was 0.57, while the potential difference $\Delta E_p (=$

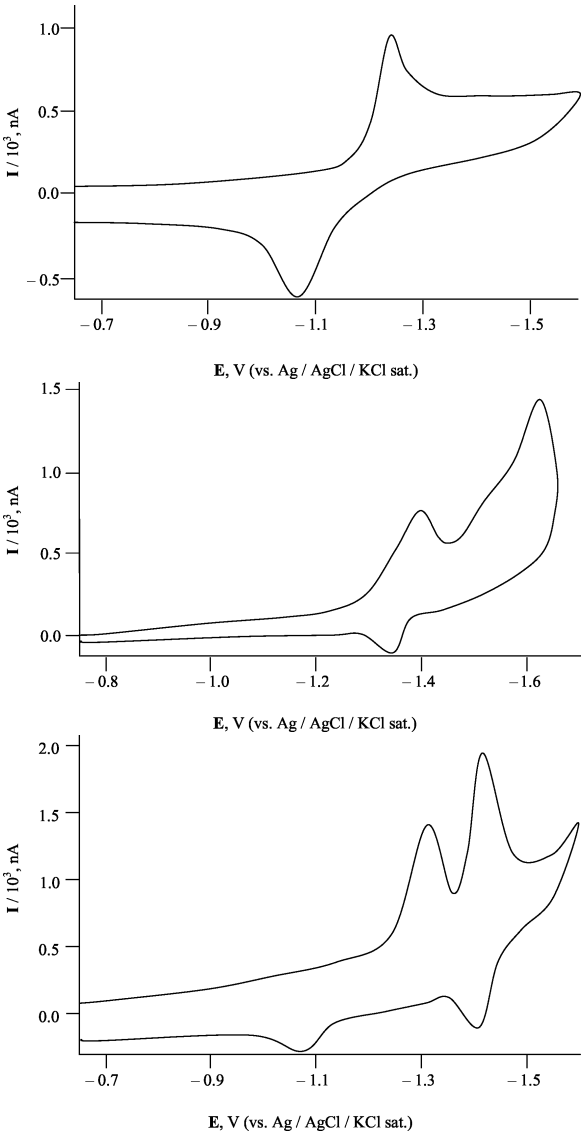

Fig. 3. Top: The cyclic voltammogram of complex **1**. Middle: The cyclic voltammogram of free bpy. Bottom: The cyclic voltammogram of complex **2**.

$E_{pa} - E_{pc}$) was 37 mV ($\nu = 250$ mVs^{-1}). The bpy exhibits two cathodic waves similar to those found for N-alkylpyridinium ions, 4,4'-bipyridine and N,N'-dialkylpyridinium ions [17], but in contrast to these compounds, bpy possibly gives a quasi-reversible two-electron transfer to form a radical. Similarly, this radical is irreversibly reduced at more negative potentials.

Complex **2** yields two reduction peaks at -1.312 and -1.412 V in the cathodic branch, and two oxidation peaks at -1.052 and -1.380 V on the reverse scan (see Fig. 3). With the potential scan rate ν increasing from 100 to 1000 mVs^{-1}, the currents of the cathodic peaks increased. Moreover, the linear equations of the $\log I_p - \log \nu$ relationship for the cathodic peaks and their slope values (0.74) indicate that the reduction peaks are diffusion-controlled with adsorption contribution. The potential differences $\Delta E_p (= E_{pa} - E_{pc})$ of the peaks depend on the scan rate. The potential difference of **2** increased typically from 236 to 276 mV, while that of bpy decreased from 56 to 28 mV, with the scan rate ranging from 100 to 1000 mVs^{-1}. Furthermore, the cathodic peak potentials shift to more negative potentials with increasing scan rate. The voltammetric data indicate that the electrode process of the complexed zinc(II) ions in complex **2** is quasi-reversible and very slow. Finally, the peak at -1.412 V can be attributed to the reduction of the coordinated bpy ligands, formed from the electrode reaction of complex **2** on the mercury electrode surface.

Experimental Section

Materials and measurements

All reagents were commercially available and used without further purification. Elemental analyses (C, H, N) were carried out on an Elementar Vario EL elemental analyzer. The FT-IR spectra were recorded from KBr pellets in the range 4000 – 400 cm^{-1} by using a Mattson 100 FTIR spectrophotometer. Thermal analysis curves (TG and DTA) were obtained using a Rigaku TG8110 thermal analyzer in a static air atmosphere at a heating rate of 10 °C min^{-1}.

A three-electrode potentiostatic control system (EG&G PARC 303A SMDE) with a hanging mercury working electrode, a Ag|AgCl|KCl$_{sat.}$ reference electrode and a platinum auxiliary electrode was used in the voltammetric experiments. The potential scan was generated by means of an EG&G PAR 384B Polarographic Analyzer. The recording of current-potential curves was obtained by means of a Houston Instrument DMP-40 plotter connected to the polarograph. The stock solutions of the complexes were prepared in triply distilled and deionized water, including 20% (v/v) isopropanol, and used immediately. 0.1 M NH_3/NH_4Cl buffer (pH 9.6) was used as supporting electrolyte. Prior to the voltammetric experiments, the solution within the electrochemical cell was deaerated by purging with pure nitrogen gas for 5 min, and during measurements a stream of nitrogen gas was passed over the solution. The voltammograms were obtained by using equilibrium time of 5 s and a drop size of medium at ambient temperature. The range of potentials from -0.6 to -1.6 V was selected unless stated otherwise.

Table 4. Crystallographic data for **1** and **2**.

	1	**2**
Empirical formula	$C_{18}H_{30}N_6O_6Zn$	$C_{26}H_{32}N_6O_7Zn$
M_r	491.85	605.95
T [K]	296(2)	296(2)
Radiation, λ []	0.71073	0.71073
Crystal system	monoclinic	monoclinic
Space group	$C2/c$	$P2_1/n$
Unit cell dimensions		
a [Å]	16.6055(18)	12.5520(8)
b [Å]	11.7468(8)	19.8450(10)
c [Å]	13.4126(15)	12.6770(8)
β [°]	122.714(8)	115.721(4)
V [Å^3]	2201.3(4)	2844.9(3)
Z	4	4
D_c [g/cm^3]	1.484	1.415
μ [mm^{-1}]	1.163	0.917
F(000)	1032	1264
Crystal size [mm^3]	0.49×0.34×0.25	0.47×0.40×0.33
θ Range [°]	2.27/25.99	1.91/27.14
Index range (h, k, l)	−20/20, −14/14, −16/16	−16/16, −25/25, −16/16
Reflections collected	13806	44713
Independent reflections (R_{int})	2176 (0.0712)	6264 (0.1099)
Absorption correction	integration	integration
Min. and max. transmission	0.645 and 0.822	0.672 and 0.790
Data / parameters	2176 / 141	7467 / 369
Goodness-of-fit on F^2	1.112	1.062
Final R indices [$I > 2\sigma(I)$]	0.0355	0.0347
wR2	0.0916	0.0886
Largest diff. peak and hole [e·Å^{-3}]	0.644 and −0.409	0.274 and −0.733

Synthesis of the zinc complexes

Na(barb) (5,5-diethylbarbituric acid sodium salt) (0.82 g, 4 mmol) dissolved in water (10 ml) was mixed with $Zn(NO_3)_2$ (0.60 g, 2 mmol) dissolved in water (10 ml) with stirring. The solution immediately became milky. Ethylenediamine (en) (0.12 g, 2 mmol) was added to the milky suspension and then, addition of 10 ml of 2-propanol resulted in a clear solution. The resulting solution was stirred for 30 min at room temperature and was allowed to stand at room temperature. Colorless crystals of **1** were obtained after 2 d. Yield 85%. $C_{18}H_{30}N_6O_6Zn$ (491.85): calcd. C 43.96, H 6.15, N 17.09; found C 43.83, H 6.29, N 17.62.

Complex **2** was synthesized in a similar manner except that 2,2'-dipyridyl (bpy) was used instead of en. 2,2'-dipyridyl was dissolved in methanol. Yield 62%. $C_{26}H_{32}N_6O_7Zn$ (605.95): calcd. C 51.54, H 5.32, N 13.87; found C 51.68, H 5.47, N 14.02.

X-ray crystallography

Intensity data for complexes **1** and **2** were collected using a STOE IPDS 2 diffractometer at 296 K. The structures were solved and refined using SHELXS-97 and SHELXL-97 [18]. All non-hydrogen atoms were found on the difference Fourier map and refined anisotropically. All CH hydrogen atoms in **1** and **2** were included using a riding model. The details of data collection, refinement and crystallographic data are summarized in Table 4.

Crystallographic data have been deposited with the Cambridge Crystallographic Data Centre as supplementary publication no. CCDC-292288 (**1**) and CCDC-292290 (**2**). Copies of the data can be obtained on application to CCDC, 12 Union Road, Cambridge CB2 1EZ, UK [Fax: (internat.) + 44-1223/336-033; E-mail: deposit@ccdc.cam.ac.uk].

Acknowledgement

The authors wish to thank Ondokuz Mayis University for financial support.

[1] J. N. Delgado, W. A. Remers, J. B. Lippincott (eds): Wilson and Gisvold's Textbook of Organic Medicinal and Pharmaceutical Chemistry, 9th ed., Lippincott-Raven, Philadelphia (1991).
[2] J. J. L. Zwicker, Pharm. Weekblad **68**, 975 (1931).
[3] J. Morvay, J. Szabo, G. Kozepesy, Acta Pharm. Hung. **39**, 208 (1969).
[4] D. Craciunescu, E. Popa, A. Fruma, Israel J. Chem. **8**, 93 (1970).
[5] B. C. Wang, B. M. Craven, Chem. Commun. 290 (1971).
[6] L. Nassimbeni, A. Rodgers, Acta Crystallogr. **B30**, 1953 (1974).
[7] F. Yilmaz, V. T. Yilmaz, C. Kazak, Z. Anorg. Allg. Chem. **631**, 1536 (2005).
[8] M. R. Caira, G. V. Fazakerley, P. W. Linder, L. R. Nassimbeni, Acta Crystallogr. **B29**, 2898 (1973).
[9] B. Berking, B. M. Craven, Acta Crystallogr. **B27**, 1107 (1971).
[10] B. Berking, Acta Crystallogr. **B28**, 98 (1972).
[11] L. Levi, C. E. Hubley, Anal. Chem. **28**, 1591 (1956).
[12] P. Zuman, J. Koryta, R. Kalvoda, Coll. Czech. Chem. Commun. **18**, 350 (1953).
[13] W. Pasek, J. Volke, O. Manousek, Coll. Czech. Chem. Commun. **40**, 819 (1975).
[14] S. Berchmans, R. Vijayavalli, Electroanalysis **6**, 1063 (1994).
[15] J. Heyrovský, J. Kůta, Principles of Polarography, p. 560, Academic Press, New York (1966).
[16] L. Meites, Polarographic Techniques, p. 679, Interscience Publishers, New York (1965).
[17] P. Zuman, C. L. Perrin, Organic Polarography, p. 280, Interscience Publishers, New York (1969).
[18] G. M. Sheldrick, SHELX-97, Programs for Crystal Structure Analysis, University of Göttingen, Germany (1997).